 MCB, vol.8, no.3, pp.169-193, 2011

Cytoplasmic Motion Induced by Cytoskeleton Stretching and Its Effect on Cell Mechanics

T. Zhang*

Abstract: Cytoplasmic motion assumed as a steady state laminar flow induced by cytoskeleton stretching in a cell is determined and its effect on the mechanical behavior of the cell under externally applied forces is demonstrated. Non-Newtonian fluid is assumed for the multiphase cytoplasmic fluid and the analytical velocity field around the macromolecular chain is obtained by solving the reduced nonlinear momentum equation using homotopy technique. The entropy generation by the fluid internal friction is calculated and incorporated into the entropic elasticity based 8-chain constitutive relations. Numerical examples showed strengthening behavior of cells in response to externally applied mechanical stimuli. The spatial distribution of the stresses within a cell under externally applied fluid flow forces were also studied.

Keywords: cell cytoplasm cytoskeleton macromolecules non-Newtonian fluid constitutive relation

1 Introduction

Cytoplasmic motion could be induced by macromolecular chain stretching in a cell. For example, in amoeboid movement, contraction due to the interaction of actin filaments with myosin near cell's trailing end squeezes the fluid forward into the pseudopodium; in plant cells, cytoplasmic streaming, a circular flow of cytoplasm within cell, could be brought by actin-myosin contraction and sol-gel transformations; in adherent cells, fluid motion could be formed during stress fibers assembly and disassembly. Cytoplasmic fluid dynamics, transport, and interaction with cytoskeletal network have been studied in numerous publications [1, 2, 3, 4, 5]. In the current paper, we focus on the steady state laminar flow in cytoplasmic motion and one-way interaction between cytoskeletal filaments and cytoplasmic motion. that

* Corresponding author. Institute of Northern Engineering, University of Alaska Fairbanks 306 Tanana Drive, Duckering Building, Fairbanks, AK99775-5910. tzhang@alaska.edu

is, cytoskeletal filaments induce cytoplasmic fluid flow. Such flow could occur in cytoplasmic streaming, amoeboid movement, and around bundled stress fibers.

Cytoplasmic fluid, cytosol, make up ∼70% of the total volume of a typical cell and 20-30% of which is occupied by different macromolecules with viscosity being 5-20 times that of water. Cytoplasmic fluid, therefore, can be considered as multiphase fluid, a mixture of solid particles entrained in a fluid. Multiphase fluid flow has found broad applications in industries and engineering such as microalgae in photobioreactors, particulate matter in exhaust emission, and solids in industrial waste stream, etc. Such a fluid-solid mixture displays complicated physical, chemical, and mechanical behavior depending on numerous variables, e.g., geometry of the particles, physical, chemical, and mechanical properties of each constituent, and their volume fractions.

One possible approach to model the fluid-solid mixture is to consider each phase as a single individual continuum with its own governing equations, interacting with each other through coupled equations [6, 1, 7, 8, 2]. Alternatively, the fluid-solid mixture is considered as a single homogeneous continuum behave as a non-Newtonian fluid. Such an approach has been used by numerous authors to obtain approximate analytical solutions for pipe flow [9, 10, 11, 12], parallel plate flow [13], channel flows [14], and torsional flow [15]. Here, we consider cytosol as a non-Newtonian fluid, its motion induced by macromolecular chain stretching, and the effect on cell mechanics. An approximate analytical solution of the velocity field is firstly obtained for cytoplasmic motion. The entropy generated by the fluid motion is then incorporated into the entropic elasticity based constitutive models to describe the mechanical behavior of cells under externally applied forces.

2 Governing equations

The constitutive relation of non-Newtonian fluid was given by Rivlin and Ericksen [16] as

$$T = -pI + \mu A_1 + \alpha_1 A_2 + \alpha_2 A_1^2 + \beta_1 A_3 + \beta_2 [A_1 A_2 + A_2 A_1] + \beta_3 [tr(A_1^2)] A_1 \tag{1}$$

where μ is the viscosity coefficient; α_1, α_2, β_1, β_2, and β_3 are material parameters that are generally temperature dependent. T is the stress tensor and pI the spherical stress tensor. The kinematic tensors $A_k (k = 1, 2, 3)$ are defined by the velocity field $\bar{v}$ as

$$A_1 = \nabla \bar{v} + \bar{v} \nabla \tag{2a}$$

$$A_n = \frac{d}{dt} A_{n-1} + A_{n-1} \nabla \bar{v} + \bar{v} \nabla A_{n-1}, \qquad n = 2, 3 \tag{2b}$$

where ∇ is gradient operator and $\frac{d}{dt}$ is the material time derivative. It has been shown [17] that for thermodynamically compatible fluid the constitutive relation Eq. (1) can be reduced to

$$T = -pI + [\mu + \beta_3[tr(A_1^2)]A_1 + \alpha_1 A_2 + \alpha_2 A_1^2. \tag{3}$$

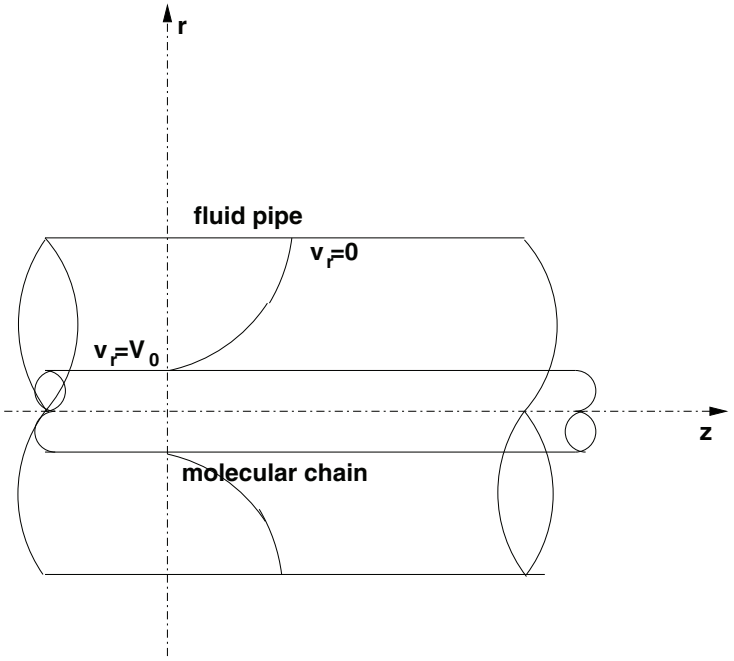

Figure 1: Diagram of surrounding fluid pipe concentrated with a macromolecular chain.

Considering the diameter is about 1.0 nm for macromolecular chain and 1-10 μm for cells, the fluid motion induced by chain stretching should be localized. For the localized fluid motion, we only consider laminar flow surrounding a single chain and ignore the flow interaction among different chains. This assumption serves the purpose to include the effect of fluid motion in the cell constitutive relation rather than to conduct a full scale fluid dynamics analysis and interaction with the cytoskeleton. Under such assumption, the surrounding fluid moves with the chain and forms a concentric fluid pipe with macromolecular chain as shown in Fig. 1. Suppose there is no sliding between the fluid and the chain, the inner boundary of the fluid pipe has the same velocity, V_0, as the chain moves. The velocity on the

outer boundary is zero. Following Massoudi and Christie's work [9] for pipe flow, the governing equation for the current problem is given by

$$\frac{d}{dr}\left(r\frac{dv}{dr}\right)+\Lambda\left(\frac{dv}{dr}\right)^2\left(\frac{dv}{dr}+3r\frac{d^2v}{dr^2}\right)=C \tag{4a}$$

$$(v)_{r=\frac{R}{1-R}}=1 \text{ and } (v)_{r=\frac{1}{1-R}}=0 \tag{4b}$$

where $r=\frac{\bar{r}}{R^*}$, $v=\frac{\bar{v}}{V_0}$, $R^*=\bar{r}_0-\bar{r}_i$, $\Lambda=\frac{2\beta_3 V_0^2}{\mu_* R^{*2}}$, $R=\frac{\bar{r}_i}{\bar{r}_o}$, $\bar{r}_i$, and $\bar{r}_o$ are the inner and outer radius of the fluid pipe, respectively, μ_* is a reference fluid viscosity, and $C=0$ is the pressure differential in the pipe. Here we have assumed that both viscosity coefficient and pressure along axial direction are constants. Obviously, equation (4) is a nonlinear ordinary differential equation. Perturbation and homotopy methods have been often used to solve such equations. Here, we use homotopy method [18] to solve the nonlinear problem of Eq. (4).

3 Homotopy method

In general, a nonlinear differential equation of a unknown function u can be written as

$$\mathscr{A}(u)-f(r)=0, \qquad r\in\Omega \tag{5}$$

with boundary conditions

$$\mathscr{B}(u,\frac{\partial u}{\partial n})=0, \qquad r\in\Gamma \tag{6}$$

where $\mathscr{A}$ is a general differential operator, $f(r)$ is a known analytical function, $\mathscr{B}$ is a boundary operator, $\frac{\partial u}{\partial n}$ is the gradient of u along the normal direction n of the boundary Γ that encloses the domain Ω. $\mathscr{A}$ can be divided into linear and nonlinear operators, $\mathscr{L}$ and $\mathscr{N}$, respectively. Equation (5) can then be written as

$$\mathscr{L}(u)+\mathscr{N}(u)-f(r)=0. \tag{7}$$

A homotopy $v(r,p):\Omega\times[0,1]\to\mathscr{R}$ can be constructed and satisfies

$$\mathscr{H}(v,p)=(1-p)[\mathscr{L}(v)-\mathscr{L}(u_0)]+p[\mathscr{A}(v)-f(r)]=0 \tag{8a}$$

or

$$\mathscr{H}(v,p)=\mathscr{L}(v)-\mathscr{L}(u_0)+p\mathscr{L}(u_0)+p[\mathscr{N}(v)-f(r)]=0 \tag{8b}$$

$$p\in[0,1], \qquad r\in\Omega$$

where p is an embedding parameter, u_0 is an initial approximate solution to the original problem of Eq. (5) and satisfies the given boundary conditions.

We use a power series to approximate the solution in Eq. (8), i.e.,

$$v = v_0 + pv_1 + p^2 v_2 + \cdots \tag{9}$$

For $p = 1$, equation (8) returns to the differential equation of the original problem, i.e.,

$$\mathscr{H}(v,1) = \mathscr{A}(v) - f(r) = 0, \tag{10}$$

and Eq. 9 becomes the approximate solution of the original problem, i.e.,

$$u = \lim_{p\to 1} v = v_0 + v_1 + v_2 + \cdots. \tag{11}$$

4 Approximate analytical solution

4.1 General solution

To apply the homotopy technique, the governing equation (4) is firstly separated into linear and nonlinear operators, i.e.,

$$\mathscr{L}(u) = \frac{d}{dr}\left(r\frac{du}{dr}\right) \tag{12a}$$

$$\mathscr{N}(u) = \Lambda\left(\frac{du}{dr}\right)^2\left(\frac{du}{dr} + 3r\frac{d^2u}{dr^2}\right). \tag{12b}$$

Introducing Eqs. (9), (12a), and (12b) into Eq. (8) and collecting common terms in the order of parameter p, we obtain solutions of Eq. (8) for different orders below:

$$p\left[\frac{d}{dr}\left(r\frac{dv_1}{dr}\right) + \frac{d}{dr}\left(r\frac{dv_0}{dr}\right) + \Lambda\left(\frac{dv_0}{dr}\right)^2\left(\frac{dv_0}{dr} + 3r\frac{d^2v_0}{dr^2}\right)\right] = 0 \tag{13}$$

$$p^2\left\{\frac{d}{dr}\left(r\frac{dv_2}{dr}\right) + \Lambda\left[\left(\frac{dv_0}{dr}\right)^2\left(\frac{dv_1}{dr} + 3r\frac{d^2v_1}{dr^2}\right) + 2\frac{dv_0}{dr}\frac{dv_1}{dr}\left(\frac{dv_0}{dr} + 3r\frac{d^2v_0}{dr^2}\right)\right]\right\} = 0 \tag{14}$$

$$p^3\left\{\frac{d}{dr}\left(r\frac{dv_3}{dr}\right) + \Lambda\left[\left(\frac{dv_0}{dr}\right)^2\left(\frac{dv_2}{dr} + 3r\frac{d^2v_2}{dr^2}\right) + 2\frac{dv_0}{dr}\frac{dv_1}{dr}\left(\frac{dv_1}{dr} + 3r\frac{d^2v_1}{dr^2}\right) + \left(2\frac{dv_0}{dr}\frac{dv_2}{dr} + \left(\frac{dv_1}{dr}\right)^2\right)\left(\frac{dv_0}{dr} + 3r\frac{d^2v_0}{dr^2}\right)\right]\right\} = 0 \tag{15}$$

.....

We use

$$u_0 = \left(r - \frac{1}{R_s}\right)^2 \tag{16}$$

as the initial approximate solution with $R_s = 1 - R$, which is also the zeroth-order solution. Introducing the zeroth-order solution into Eq. (13), we obtain the first-order solution. We then use the zeroth-order and first-order solution to find the second-order solution and so on so forth until a satisfied approximate solution is obtained. The solutions for the first three orders are described below.

— *First-order solution*
Introducing Eq. (16) into Eq. (13) and integrating the resulting ordinary differential equation, we obtain the first-order solution as

$$v_1 = -\left(r - \frac{1}{R_s}\right)^2 - 2\Lambda\left(r - \frac{1}{R_s}\right)^4 + \frac{1+2\Lambda}{ln(R)} ln(R_s r). \tag{17}$$

— *Second-order solution*
Based on the zeroth-order and the first-order solutions, we obtain the second-order solution by integrating Eq. (14) as

$$\begin{aligned} v_2 = 24\Lambda \Bigg[& \frac{1}{4}\left(r - \frac{1}{R_s}\right)^4 + \frac{2}{3}\left(r - \frac{1}{R_s}\right)^6 - \frac{C_0}{4} r \left(r - \frac{4}{R_s}\right) \\ & - \frac{C_0}{2R_s^2} ln(r) \Bigg] + C_2 ln(r) + C_3 \end{aligned} \tag{18}$$

where C_0, C_2, and C_3 are integration constants defined by

$$\begin{aligned} C_0 &= \frac{1+2\Lambda}{ln(R)} \\ C_2 &= \frac{24\Lambda}{ln(R)} \left[\frac{C_0}{4R_s}(3-R) + \frac{C_0}{2R_s^2} ln(R) - \left(\frac{1}{4} - \frac{2}{3}\Lambda\right) \right] \\ C_3 &= C_2 ln(R_s) - \frac{24 C_0 \Lambda}{4R_s^2} \left[3 + 2ln(R_s)\right]. \end{aligned}$$

— *Third-order solution*
Base on zeroth-order, first-order, and second-order approximate solutions,

the third-order approximate solution can be obtained by integrating Eq. 15,

$$v_3 = -8\cdot 24\Lambda^3\left(r-\frac{1}{R_s}\right)^8 - 80\Lambda^2\left(r-\frac{1}{R_s}\right)^6 - 6\Lambda\left(r-\frac{1}{R_s}\right)^4 + 240\Lambda^2 C_0\int\frac{1}{r}\left(r-\frac{1}{R_s}\right)^4 dr - 12(C_2-2C_0)\Lambda\int\frac{1}{r}\left(r-\frac{1}{R_s}\right)^2 dr - \frac{6C_0^2\Lambda}{R_s r} + C_4 ln(r) + C_5 \quad (19)$$

where the integration constants C_4 and C_5 are given by

$$C_{4_1} = (192\Lambda^2 + 80\Lambda + 6)$$
$$C_{4_2} = -240\frac{C_0\Lambda}{R_s^4}\left[ln(R) - \frac{R_s}{12}(3R^3 - 13R^2 + 23R - 25)\right]$$
$$C_{4_3} = \frac{12}{R_s^2}(C_2 - 2C_0)\left[\frac{R_s}{2}(3-R) + ln(R)\right]$$
$$C_{4_4} = 6C_0^2\left[\frac{R_s}{R} + ln(R)\right]$$
$$C_4 = \frac{\Lambda}{ln(R)}(C_{4_1} + C_{4_2} + C_{4_3} + C_{4_4})$$
$$C_{5_1} = 240\frac{C_0\Lambda}{R_s^4}\left[\frac{25}{12} + ln(R_s)\right]$$
$$C_{5_2} = -\frac{12}{R_s^2}(C_2 - 2C_0)(\frac{3}{2} + ln(R_s)) + 6C_0^2\left[1 - ln(R_s)\right]$$
$$C_5 = \Lambda(C_{5_1} + C_{5_2}) + C_4 ln(R_s).$$

4.2 Convergence study

Whether the approximation of Eq. (9) will be considered as a solution to the original problem Eq. (5) depends on whether it converges or not as $p \to 1$. A general discussion of convergence requirements was given by He [18]. Here, for this particular case, we exam the convergence of the solution and applicable range of the parameters numerically.

Up to the seventh-order analytical solutions have been obtained to exam the convergence of the solutions numerically. The typical results are shown in Figs. 2 and 3 for the case of $\Lambda = 0.125$ and $R = 0.15$ and $\Lambda = 0.1$ and $R = 0.2$. The convergence of the solution to Eq. (5) depends on Λ and R. From the numerical study, we found that the applicable range of the obtained solution are $\Lambda \leq 0.125$ and $0.1 \leq R \leq 0.35$.

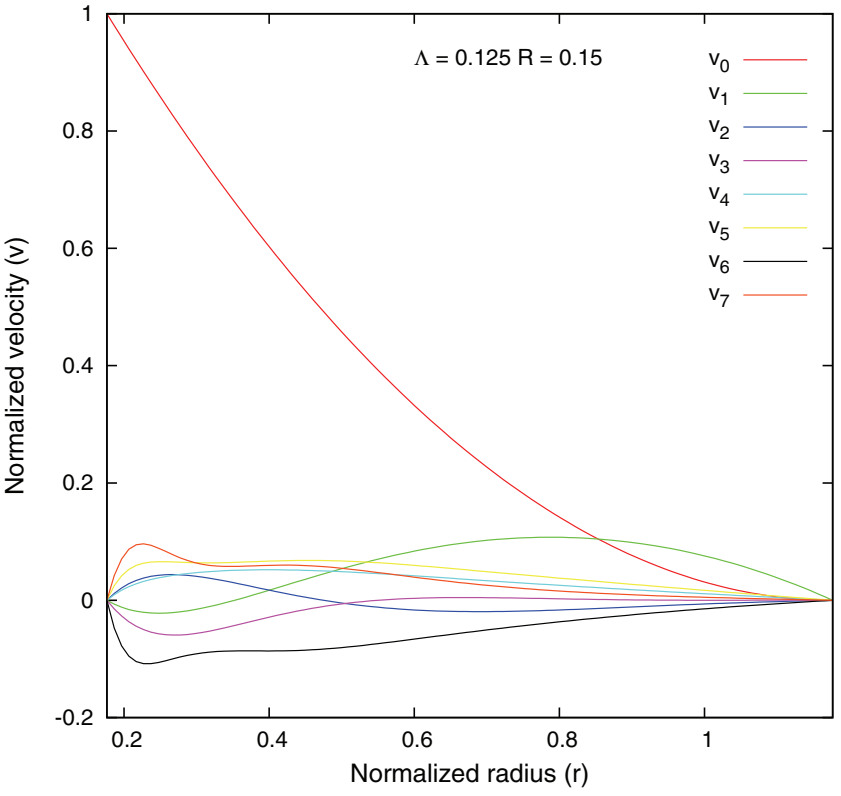

Figure 2: Normalized velocity field for different order approximation for the case $\Lambda = 0.125$ and $R = 0.15$.

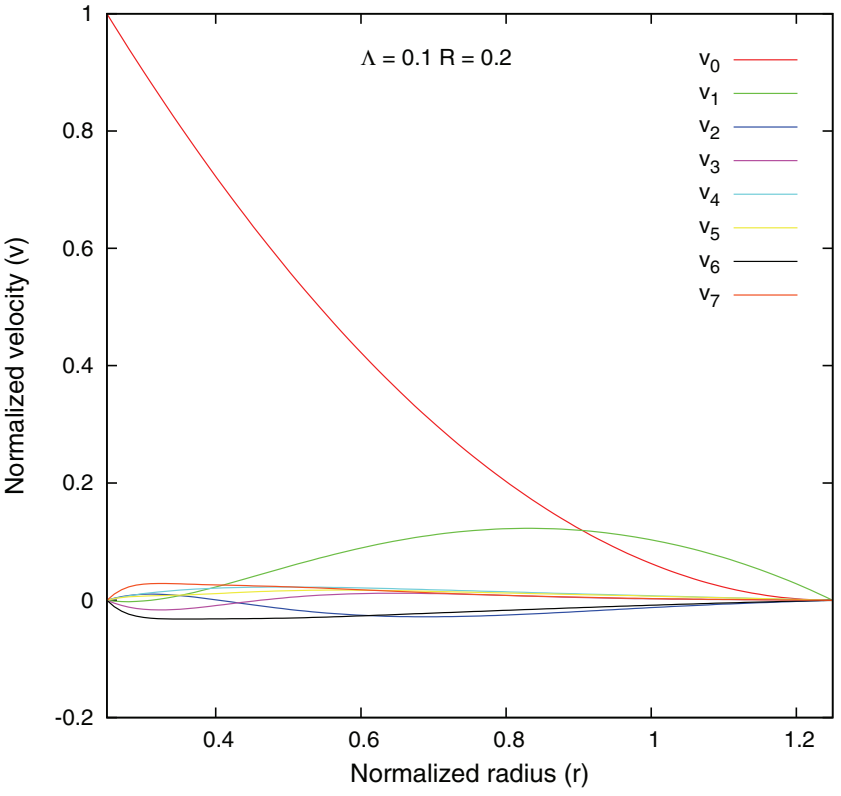

Figure 3: Normalized velocity field for different order approximation for the case $\Lambda = 0.1$ and $R = 0.2$.

We will use the third-order approximate solution to study the velocity field around the macromolecular chain in the following discussion.

5 Results and discussion

5.1 Fluid analysis

Velocity field of the fluid for three cases $R = 0.1$, 0.125, and 0.15 are analyzed for Λ ranges from 0.01 to 0.225 as shown in Figs. 4-6. The velocity field forms into two zones within the fluid pipe. The velocity near the inner boundary of the fluid pipe decreases as Λ increases. The velocity gradient within this zone decreases with the increase of R. The decreases in the velocity gradient contradicts with the zeroth-order solution where the gradient increases with R. The reason for this contradiction could be caused by the nonlinearity in the velocity field along radial direction. As shown in Figs. 4 -6, the velocity do increase with R along radial direction, however, the nonlinearity in the velocity field leads to the gradient decrease with R near the inner boundary. The velocity within the zone near the outer boundary increases with the increase of Λ. These results indicate that the magnitude of velocity field tends to extend from inner boundary toward outer boundary as R increases.

5.2 Entropy generation

The fluid motion induced by macromolecular chain stretching causes energy dissipation due to internal friction and generation of entropy. The volumetric entropy generation by the fluid flow around the macromolecular chain can be calculated by [19]

$$\dot{S} = \frac{\mu_* V_0^2}{R^{*2}\theta_0}\left(\frac{dv}{dr}\right)^2\left[\mu + \Lambda\left(\frac{dv}{dr}\right)^2\right] = \eta_s \dot{\rho}^2 V_r \tag{20}$$

in which we used

$$V_0 = \dot{\rho} L_0, \qquad \eta_s = \frac{\mu_s L_0^2}{R^{*2}\theta_0}, \qquad V_r = \left(\frac{dv}{dr}\right)^2\left[\mu + \Lambda\left(\frac{dv}{dr}\right)^2\right],$$

where $\dot{\rho}$ is chain stretching rate, L_0 is the macromolecular chain length, θ_0 is ambient temperature.

6 Application in cell mechanics

6.1 Constitutive relation

The macromolecular chain network model based on configurational entropy have been developed to describe large strain, nonlinear elastic deformations of polymers

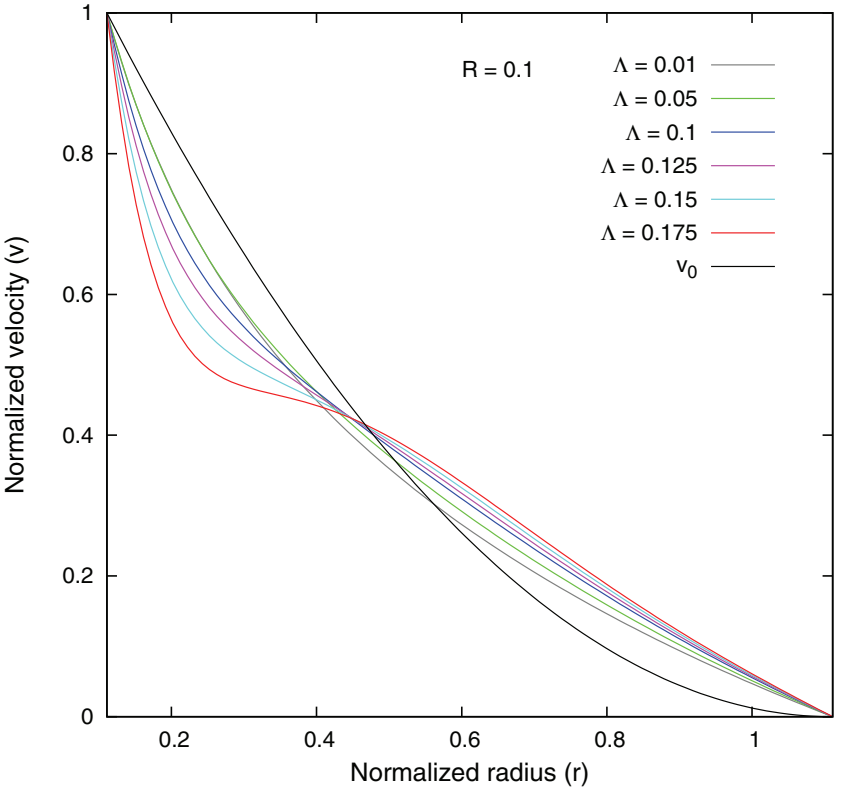

Figure 4: Fluid velocity of the fluid surrounding the chain $R = 0.1$.

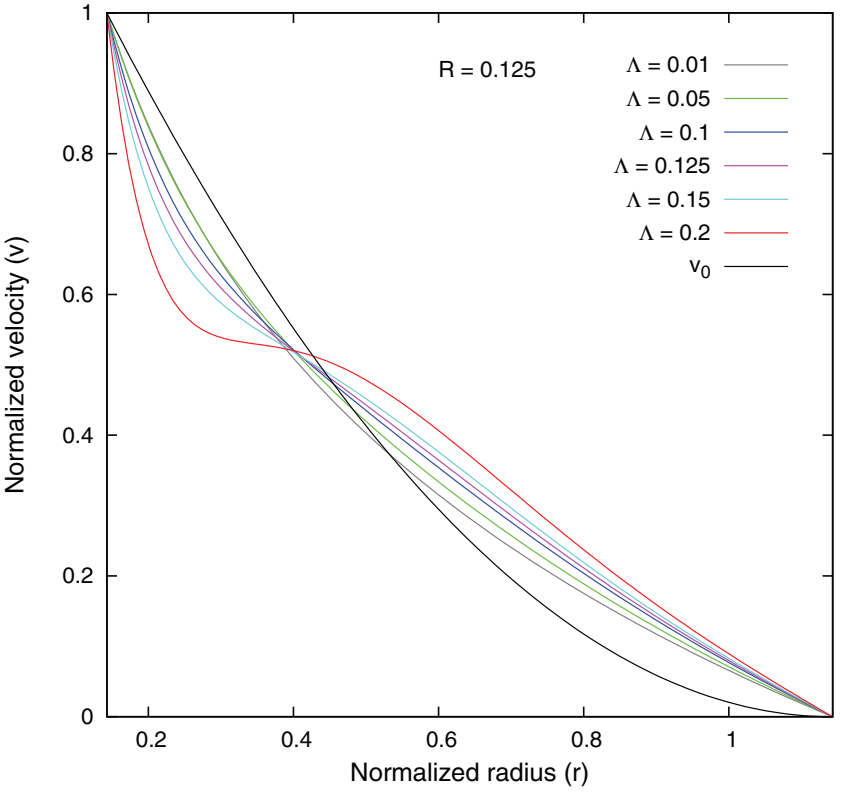

Figure 5: Normalized fluid velocity of surrounding fluid $R = 0.125$.

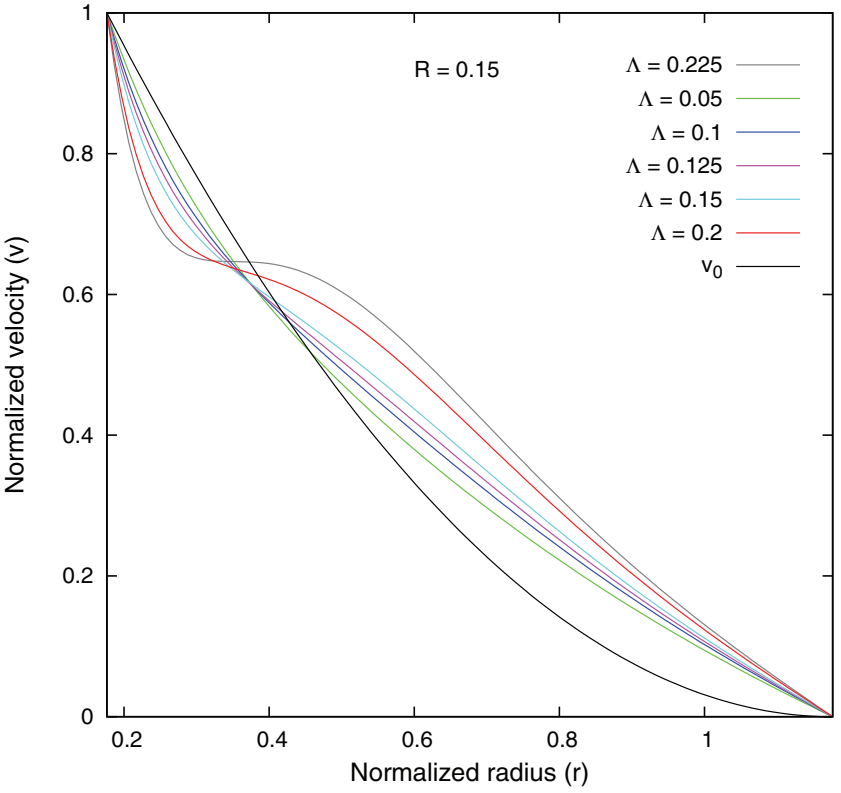

Figure 6: Normalized fluid velocity of the surrounding fluid $R = 0.15$.

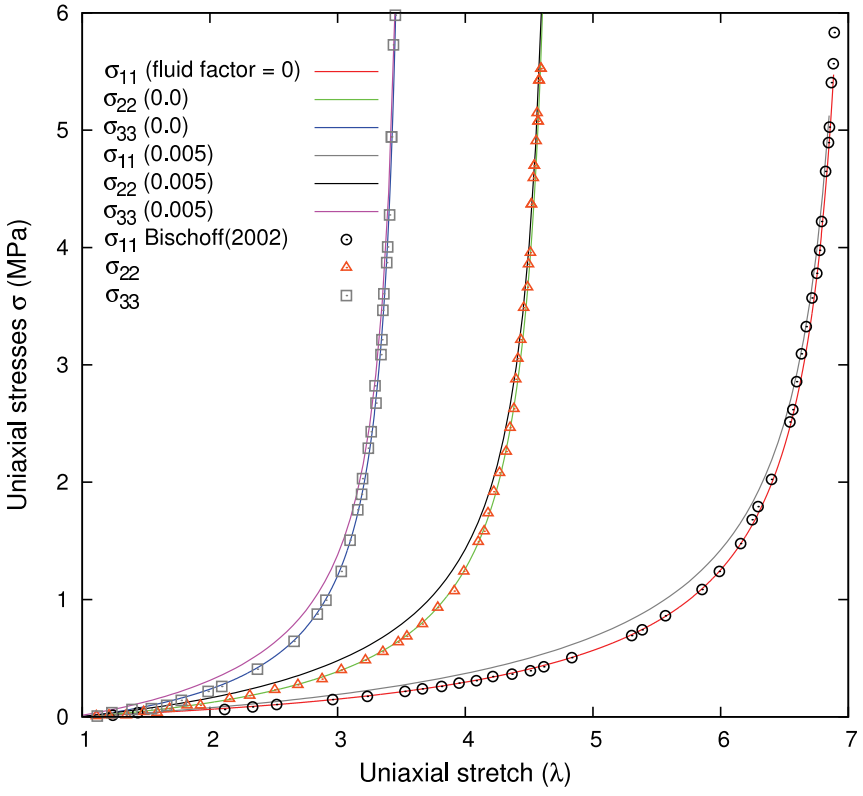

Figure 7: Uniaxial stretch versus uniaxial stresses in X_1, X_2 and X_3, respectively (fluid factor = $\eta_s V_r$).

or polymer-like materials, including "3-chain" cubic unit cell model [20], "4-chain" tetrahedral model [21, 22], and "8-chain" cubic model [23]. In addition to these isotropic network models, orthotropic and anisotropic chain network models were also proposed by Bischoff et al. [24] and Kuhl et al. [25], respectively. Here, we extend 8-chain models, both isotropic and orthotropic, to include the interaction between cytoplasmic motion and cytoskeleton in the constitutive relation to describe the mechanical behavior of cells.

6.1.1 8-chain isotropic model

The second Piola-Kirchhoff stress for the 8-chain isotropic model that includes the effect of cytoplasmic motion is given by (see Appendix)

$$S_{ji} = \frac{1}{J^{2/3}}\left(Nk\theta C_0 + \frac{2}{3}\eta_s V_r\right)\left(F_{ij} - \frac{1}{3}B_{kk}F_{ji}^{-1}\right) + KJ(J-1)F_{ji}^{-1} \tag{21}$$

where N is the chain density, k the Boltzmann's constant, θ is absolute temperature, $J = (\det \mathbf{B})^{1/2}$, $B_{ij} = F_{ik}F_{jk}$, F_{ij} is the deformation gradient, K is the bulk modulus, and

$$C_0 = \left[1 + \frac{B_{kk}}{5J^{2/3}\lambda_m^2} + \frac{33(B_{kk})^2}{525J^{4/3}\lambda_m^4} + \cdots\right]. \tag{22}$$

with λ_m being a material constant.

6.1.2 8-chain orthotropic model

The second Piola-Kirchhoff stress tensor for 8-chain orthotropic model that includes the effect of cytoplasmic motion is given by (see Appendix)

$$\begin{aligned} S_{jk} = \frac{Nk\theta}{4}\left\{\sum_{i=1}^{4}\frac{P_j^{(i)}P_k^{(i)}}{\rho^{(i)}}\beta_\rho^{(i)} - \frac{\beta_P}{\sqrt{n}}\left[\frac{a^2}{\lambda_a^2}a_j a_k + \frac{b^2}{\lambda_b^2}b_j b_k + \frac{c^2}{\lambda_c^2}c_j c_k\right]\right\} \\ + \sum_{i=1}^{4}\left\{2\theta\eta_s V_r^{(i)}P_j^{(i)}P_k^{(i)}\right\} + \frac{B}{\alpha}sinh[\alpha(J-1)]\frac{\partial J}{\partial E_{jk}} \end{aligned} \tag{23}$$

where $\rho^{(i)} = \sqrt{{P^{(i)}}^T \cdot C \cdot P^{(i)}}$, $\beta_\rho^{(i)} = \mathscr{L}^{-1}(\frac{\rho^{(i)}}{n})$, $\beta_P = \mathscr{L}^{-1}(\frac{P}{n})$, $\mathscr{L}^{-1}(x)$ is the inverse of Langevin function $\mathscr{L}(x) = coth(x) - \frac{1}{x}$, $\lambda_a = \sqrt{a^T \cdot C \cdot a}$, $\lambda_b = \sqrt{b^T \cdot C \cdot b}$, $\lambda_c = \sqrt{c^T \cdot C \cdot c}$, (a,b,c) is the dimension of the unit cell in local coordinate system, $P^{(i)}$ is chain vector in local coordinate system $(\mathbf{a},\mathbf{b},\mathbf{c})$, $a_m, b_m, c_m (m = i, j, k)$ the coordinates of (a,b,c) in global system (X_1, X_2, X_3), C is right Cauchy-Green

tensor, B is the bulk modulus of the surrounding media of the chains, α governs the curvature between pressure and volume variation, and

$$\frac{\partial J}{\partial E_{jk}} = (\varepsilon_{jyz}\delta_{1k}C_{y2}C_{z3} + \varepsilon_{xjz}C_{x1}\delta_{2k}C_{z3} + \varepsilon_{xyj}C_{x1}C_{y2}\delta_{3k})/J \tag{24}$$

in which E is Lagrangian strain tensor, ε_{ijk} permutation tensor, and δ_{ij} is Kronecker delta. Cauchy stress tensor can then be calculated by

$$T = \frac{1}{J}F \cdot S \cdot F^T. \tag{25}$$

For a special case in which local coordinate system (a,b,c) aligned with three orthotropic material orientation coincides with global reference system (X_1,X_2,X_3), the variation of the stresses with respect to principal stretch is studied to demonstrate the effects of cytoplasmic motion on the constitutive relation. The material under uniaxial stretching with and without fluid motion are analyzed and compared with the results without fluid motion given by Bischoff et al. [24]. For uniaxial case, an nonlinear equation test program - TESTNONLIN [26] is modified to include subroutines to calculate stresses. The parameter used in this case are: $a = 2$, $b = 3$, $c = 4$; $N = 8 \times 10^{24}/m^3$; $n = 7.25$; $B = 1Mpa$; and $\theta = 295^0$K. For the non-Newtonian fluid, $\mu_* \approx 4 \times 10^{-3}$ (Pa-s), $\mu = 1$, and Λ is between 0.1 - 0.125. V_r is estimated by considering the velocity gradient between 5 - 100 for Λ within [0.1, 0.15] and R within [0.1, 0.2]. In this case, we used the value of 0.005 for $\eta_s V_r$. The results for uniaxial stretch versus stresses are shown in Fig. 7. These results indicate that the cytoplasmic motion increases the magnitude of the stresses at small or medium stretch. The effect of fluid motion also depends on the unit cell geometric size a, b, and c. For example, the fluid motion increases the stress at medium stretch along X_1 direction and at small and medium stretch along X_2 and X_3 directions.

7 Example

In this example, we use the modified 8-chain constitutive model to study the mechanical response of cells under externally applied forces of fluid flow. The constitutive model was implemented into the finite element program Comsol Multiphysics 3.5a [27] to model a rotating rheometer (TA Instruments, AR-G2) which was used to measure cell adhesion strength [28]. The rheometer has two parallel plates: upper and lower which are separated by a gap of 0.48mm. The upper plate acts as a spindle rotated by a shaft controlled by a magnetic motor. The lower plate is mounted on a bench table, on top of which the cell seeded polycarbonate sample is placed. The gap is filled with PBS. The spindle is loaded on the top of the

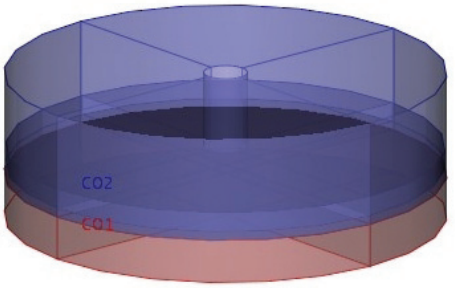

(a) Rheometer used to measure cell adhesion. The lower plate is in pink and the plate of spindle is connected with the shaft inside the blue hood.

(b) Finite element model and mesh for 2D axisymmetric fluid.The dense meshes are where the cells located.

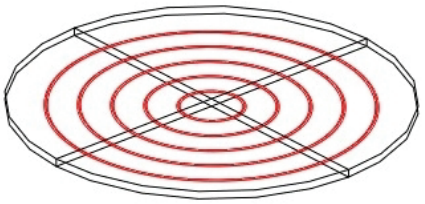

(c) Finite element model of cells (in rings). The cell density is high such that their distribution can be considered as geometrically axisymmetric.

Figure 8: Finite element model for rotational fluid flow rehometer.

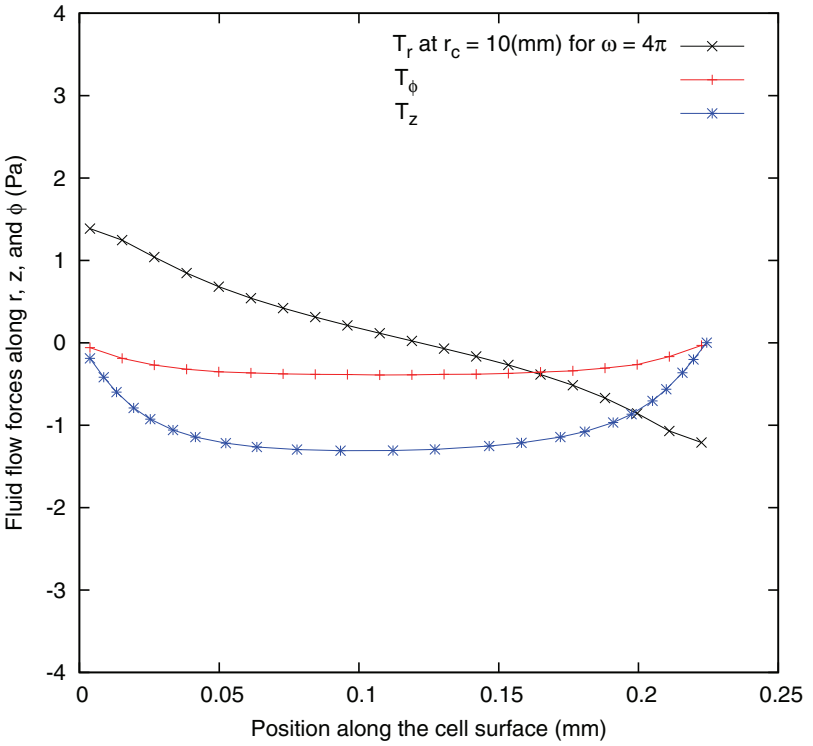

Figure 9: Wall forces due to rotational fluid flow applied on the cell surfaces in r, z, and ϕ directions at rotational velocity ω. r_c is distance of the cell center from the rotational axis.

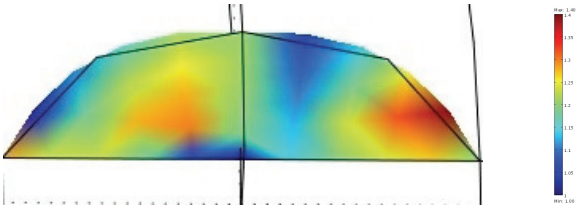

(a) σ_x (scale range is 1.0-1.4 Pa). (b)

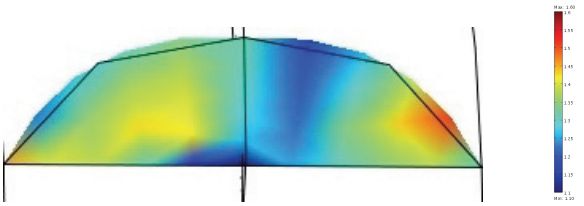

(c) σ_y (scale range is 1.1 - 1.6 Pa). (d)

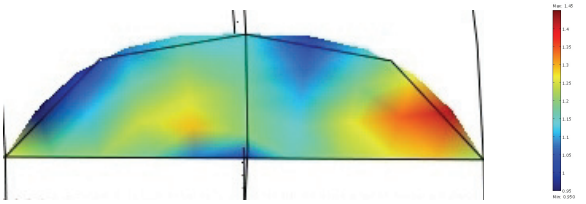

(e) σ_z (scale range is 0.95-1.45 Pa). (f)

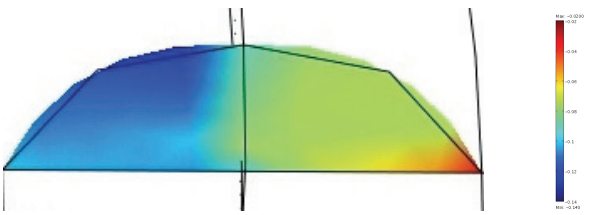

(g) σ_{xy} (scale range is -0.14 to -0.02 Pa). (h)

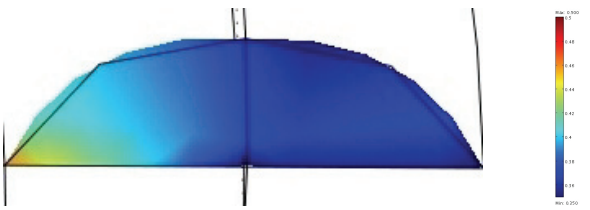

(i) σ_{yz} (scale range is 0.35-0.5 Pa). (j)

Figure 10: Stresses variation within a across section of a cell.

PBS and rotates to generate rotational flow with controllable angular shear stress as shown in Fig. 8(a).

The finite element model for the apparatus is shown in Fig. 8(b) and 8(c), The fluid flow is treated as 2-D axisymmetric swirl flow. The differential equations that describe the axisymmetric swirl flow is given in cylindrical coordinate system by

$$\begin{aligned}
\rho\left(u\frac{\partial u}{\partial r}-\frac{v^2}{r}+w\frac{\partial u}{\partial z}\right)+\frac{\partial p}{\partial r}&=\mu\left[\frac{1}{r}\frac{\partial}{\partial r}\left(r\frac{\partial u}{\partial r}\right)-\frac{u}{r^2}+\frac{\partial^2 u}{\partial z^2}\right]+F_r\\
\rho\left(u\frac{\partial v}{\partial r}-\frac{uv}{r}+w\frac{\partial v}{\partial z}\right)&=\mu\left[\frac{1}{r}\frac{\partial}{\partial r}\left(r\frac{\partial v}{\partial r}\right)-\frac{v}{r^2}+\frac{\partial^2 v}{\partial z^2}\right]+F_\phi\\
\rho\left(u\frac{\partial w}{\partial r}+w\frac{\partial w}{\partial z}\right)+\frac{\partial p}{\partial z}&=\mu\left[\frac{1}{r}\frac{\partial}{\partial r}\left(r\frac{\partial w}{\partial r}\right)+\frac{\partial^2 w}{\partial z^2}\right]+F_z
\end{aligned} \tag{26}$$

where ρ and μ are the density and the dynamic viscosity of the fluid, respectively; u, v, and w are the velocity components in r, ϕ, and z directions, respectively; p is the fluid pressure; and F_r, F_ϕ, and F_z are the components of the body forces in r, ϕ, and z directions, respectively. The viscous stress tensor and the total stress tensor are defined, respectively, by

$$\tau=\mu\left(\nabla\mathbf{u}+\mathbf{u}\nabla\right) \tag{27}$$

and

$$\sigma=-pI+\mu\left(\nabla\mathbf{u}+\mathbf{u}\nabla\right). \tag{28}$$

The finite element simulation was conducted in two steps. The first step was to obtain the external forces of fluid flow applied on the cell surfaces by carrying out 2D steady state fluid flow analysis. These forces as shown in Fig. 9 were then spanned into 3D distributions and mapped onto the 3D cell surfaces as shown in Fig. 8(c). The second step was to analyze the mechanical response of the cells under the passive forces applied by the fluid flow. The stress distributions (σ_x, σ_y, σ_z, σ_{xy}, σ_{yz}) along a cross section of a cell were shown in Figs. 10(a) to 10(j). The variation of the normal stresses σ_x, σ_y, and σ_z are quite similar and the magnitude are close. The variation of the magnitude of these normal stresses is about 0.5 Pa. The variation of the magnitude of shear stresses τ_{xy} and τ_{yz} is about 0.15 Pa.

8 Conclusion

The reduced nonlinear equation from fluid momentum equation and the constitutive relation of non-Newtonian fluid can be solved analytically for cytoplasmic motion

induced by macromolecular chain stretching using homotopy method. The velocity field around macromolecular chain forms two zones with different flow patterns that depend on spatial dimension and the properties of non-Newtonian fluid. The velocity gradient near the inner boundary decreases with the decrease of the thickness of the fluid pipe, which could be caused by the nonlinearity of the velocity field. The drag due to the fluid motion, represented by the entropy generation in this case, strengthens the cytoskeleton response to external forces. Incorporation of the interaction between cytoplasmic motion and cytoskeleton into the constitutive relation improves the model capability in studying cell motility, amoeboid movement, cytoplasmic streaming, and cell adhesion which are important in the development of biomaterials, bioenergy, and biotechnology.

Appendix A. 8-chain isotropic model

The 8-chain isotropic model characterizes the macromolecular network with a cubic unit cell consisting of 8 chains arranged diagonally and deformed with the unit cell [23] and the cytoplasmic fluid. The rate form of the strain energy function consists of the part due to configurational entropy of the chains and the part due to the fluid motion induced entropy, i.e.,

$$\dot{W} = \dot{W}_{8ch} + \theta \dot{S}_{fluid} = \frac{\partial W_{8ch}}{\partial F_{ij}} \frac{dF_{ij}}{dt} + \theta \dot{S}_{fluid}. \tag{A-1}$$

where $\dot{S}_{fluid}$ is given in Eq. 20.

The strain energy function due to configurational entropy can be simply expressed as [23]

$$W_{8ch} = Nk\theta\sqrt{n}\left\{\beta_{chain}\lambda_{chain} + \sqrt{n}\,ln\left[\frac{\beta_{chain}}{\sinh(\beta_{chain})}\right]\right\} + \frac{K}{2}(J-1)^2 \tag{A-2}$$

in which n the number of rigid links in a chain, $\beta_{chain} = \mathscr{L}^{-1}\left(\frac{\lambda_{chain}}{\sqrt{n}}\right)$, $\lambda_{chain} = \frac{1}{\sqrt{3}}\left(\lambda_1^2+\lambda_2^2+\lambda_3^2\right) = \sqrt{\frac{I_1}{3}}$ is the stretch of each chain expressed as the stretch of the unit cell, and K bulk modulus.

By Taylor expansion of β_{chain}, the strain energy function can be approximated by

$$W_{8ch} = \sum_{i=1}^{n} C_i\left(I_1^i - 3^i\right) + \frac{K}{2}(J-1)^2 \tag{A-3}$$

where C_i are determined a priori as functions of the material properties n and N.

Since $\bar{I}_1 = I_1/J^{2/3}$ and $I_1 = B_{kk}$, we have

$$\dot{\bar{I}}_1 = \frac{d\bar{I}_1}{dt} = \frac{\partial \bar{I}_1}{\partial F_{ij}} \frac{dF_{ij}}{dt} = \frac{\partial \bar{I}_1}{\partial F_{ij}} \dot{F}_{ij}, \tag{A-4}$$

and

$$\dot{S}_{fluid} = \eta_s \frac{\dot{\bar{I}}_1}{3} V_r = \frac{\eta_s}{3} V_r \frac{\partial \bar{I}_1}{\partial F_{ij}} \dot{F}_{ij}. \tag{A-5}$$

The rate form of strain energy function Eq. A-1 can be rewritten as

$$\dot{W}_{8ch} = \left(\frac{\partial W_{8ch}}{\partial F_{ij}} + \frac{\eta_s}{3} V_r \frac{\partial \bar{I}_1}{\partial F_{ij}} \right) \dot{F}_{ij} = \left({}_R S_{ji} + {}_D S_{ji} \right) \dot{F}_{ij} = S_{ij} \dot{F}_{ij}. \tag{A-6}$$

Considering

$$\begin{aligned} {}_R S_{ji} = {} & \frac{Nk\theta}{J^{2/3}} \left[1 + \frac{B_{kk}}{5J^{2/3}\lambda_m^2} + \frac{33(B_{kk})^2}{525J^{4/3}\lambda_m^4} + \cdots \right] \\ & \times \left(F_{ij} - \frac{1}{3} B_{kk} F_{ji}^{-1} \right) + KJ(J-1) F_{ji}^{-1} \end{aligned} \tag{A-7a}$$

and

$$\frac{\partial \bar{I}_1}{\partial F_{ij}} = \frac{2}{J^{2/3}} \left(F_{ij} - \frac{1}{3} B_{kk} F_{ji}^{-1} \right), \tag{A-7b}$$

we obtain the second Piola-Kirchhoff stresses

$$S_{ji} = \frac{\theta}{J^{2/3}} \left(NkC_0 + \frac{2}{3} \eta_s V_r \right) \left(F_{ij} - \frac{1}{3} B_{kk} F_{ji}^{-1} \right) + KJ(J-1) F_{ji}^{-1}. \tag{A-8}$$

Appendix B. 8-chain orthotropic model

The rate form of strain energy function for the 8-chain orthotropic model consists of two parts: rate form of the strain energy function from Bischoff's model [24] and entropy generation induced by fluid motion, i.e.,

$$\dot{W} = \dot{W}_{8ch} + \dot{W}_D = \frac{\partial W_{8ch}}{\partial E} : \dot{E} + \theta \dot{S} = {}_R S : \dot{E} + {}_D S : \dot{E} = S : \dot{E}. \tag{B-1}$$

W_{8ch} consists of three components: configurational entropy of the chains ($W_{entropy}$), the interchain repulsive energy ($W_{repulsive}$), and the bulk strain energy of the isotropic

interstitial fluid (W_{bulk}) [24], i.e.,

$$\begin{aligned} W &= W_{\text{entropy}} + W_{\text{repulsive}} + W_{\text{bulk}} \\ &= W_0 + \frac{Nk\theta}{4}\left\{ n\sum_{i=1}^{4}\left[\frac{\rho^{(i)}}{n}\beta_\rho^{(i)} + ln\left(\frac{\beta_\rho^{(i)}}{\sinh(\beta_\rho^{(i)})}\right)\right] \right. \\ &\quad \left. -\frac{\beta_P}{\sqrt{n}} ln(\lambda_a^{a^2}\lambda_b^{b^2}\lambda_c^{c^2})\right\} + \frac{B}{a^2}\{\cosh[\alpha(J-1)]-1\} \end{aligned} \tag{B-2}$$

in which W_0 is the reference strain energy. ${}_RS$ is then given by

$$\begin{aligned} {}_RS_{jk} &= \frac{Nk\theta}{4}\left\{\sum_{i=1}^{4}\frac{P_j^{(i)}P_k^{(i)}}{\rho^{(i)}}\beta_\rho^{(i)} - \frac{\beta_P}{\sqrt{n}}\left[\frac{a^2}{\lambda_a^2}a_j a_k + \frac{b^2}{\lambda_b^2}b_j b_k + \frac{c^2}{\lambda_c^2}c_j c_k\right]\right\} \\ &\quad + \sum_{i=1}^{4}\left\{2\theta\eta_s V_r^{(i)}P_j^{(i)}P_k^{(i)}\right\} + \frac{B}{\alpha}sinh[\alpha(J-1)]\frac{\partial J}{\partial E_{jk}}. \end{aligned} \tag{B-3}$$

For the rectangular prism unit cell, the second part of the rate form of strain energy function is given by

$$\dot{W}_D = \theta\dot{S} = \frac{\mu_* L_0^2}{R^*}\sum_{i=1}^{4}\left[\dot{\rho}^{(i)}\right]^2\left(\frac{dv^{(i)}}{dr^{(i)}}\right)^2\left[\mu + \Lambda\left(\frac{dv^{(i)}}{dr^{(i)}}\right)^2\right]. \tag{B-4}$$

Considering $[\dot{\rho}^{(i)}]^2 = 2P_j^{(i)}P_k^{(i)}\dot{E}_{jk}$, we

$$\dot{W}_D = \frac{\mu_* L_0^2}{R^*}\sum_{i=1}^{4}P_j^{(i)}P_k^{(i)}E_{jk}\left(\frac{dv^{(i)}}{dr^{(i)}}\right)^2\left[\mu + \Lambda\left(\frac{dv^{(i)}}{dr^{(i)}}\right)^2\right] = {}_DS\colon\dot{E}. \tag{B-5}$$

where

$${}_DS_{jk} = \frac{\mu_* L_0^2}{R^*}\sum_{i=1}^{4}P_j^{(i)}P_k^{(i)}V_r^{(i)}. \tag{B-6}$$

The second Piola-Kirchhoff stress tensor $S = {}_RS + {}_DS$ is given by

$$\begin{aligned} S_{jk} &= \frac{Nk\theta}{4}\left\{\sum_{i=1}^{4}\frac{P_j^{(i)}P_k^{(i)}}{\rho^{(i)}}\beta_\rho^{(i)} - \frac{\beta_P}{\sqrt{n}}\left[\frac{a^2}{\lambda_a^2}a_j a_k + \frac{b^2}{\lambda_b^2}b_j b_k + \frac{c^2}{\lambda_c^2}c_j c_k\right]\right\} \\ &\quad + \sum_{i=1}^{4}\left\{2\theta\eta_s V_r^{(i)}P_j^{(i)}P_k^{(i)}\right\} + \frac{B}{\alpha}sinh[\alpha(J-1)]\frac{\partial J}{\partial E_{jk}}. \end{aligned} \tag{B-7}$$

References

1. Dembo, M., Harlow, F. (1986) Cell motion, contractile network, and the physics of interpenetrating reactive flow. Biophys J, 50:109-121.

2. Alt, W., Dembo, M. (1999) Cytoplasm dynamics and cell motion: two-phase flow models. Math Biosci, 156:207-228.

3. Gracheva, M.E., Othmer, H.G. (2004) A continuum model of motility in amoeboid cells. Bull Math Biol, 66:167-193.

4. Goldstein, R.E., Tuval, I., van de Meent, J.W. (2008) Microfluidics of cytoplasmic streaming and its implications for intracellular transport. Proc Natl Acad Sci USA, 105(10):3663-3667.

5. van de Meent, J.W., Sederman, A.J., Gladden, L.F., Goldstein, R.E., Tuval, I. (2010) Measurement of cytoplasmic streaming in single plant cells by magnetic resonance velocimetry. J Fluid Mech, 642:5-14.

6. Ahmadi, G. (1985) A generalized continuum theory for multiphase suspension flows. Int J Eng Sci, 23(1): 1-25.

7. Johnson, G., Massoudi, M., Rajagopal, K.R. (1991) Flow of a fluid infused with solid particles through a pipe. Int J Eng Sci, 29(6):649-661.

8. Johnson, G., Massoudi, M., Rajagopal, K.R. (1991) Flow of a fluid-solid mixture between flat plates. Chem Eng Sci, 46:1713-1723.

9. Massoudi, M., Christie, I. (1995) Effects of variable viscosity and viscous dissipation on the flow of a third grade fluid in a pipe. Int J Non Lin Mech, 30(5):687-699.

10. Yurusoy, M., Pakdemirli, M. (2002) Approximate analytical solutions for the flow of a third-grade fluid in a pipe. Int J Non Lin Mech, 37:187-195.

11. Yurusoy, M. (2004) Flow of a third grade fluid between concentric circular cylinders. Math Comput Appl, 9(1):11-17.

12. Shafieenejad, I., Moallemi, N., Afshari, H.H., Novinzadeh, A.B. (2009) Application of He's homotopy perturbation method for pipe flow of non-Newtonian fluid. Adv Studies Theor Phys, 3(5):199-211.

13. Erbay, L.B., Ercan, M.S., Sulus, B., Yalcm, M.M. (2003) Entropy generation during fluid flow between two parallel plates with moving bottom plate. Entropy, 5:506-518.

14. Roohi, E., Kharazmi, S., Farjami, Y. (2009) Application of the homotopy method for analytical solution of non-Newtonian channel flows. Phys Scr, 79:1-7.

15. Siddiqui, A.M., Haroon, T., Irum, S. (2009) Torsional flow of third grade fluid using modified homotopy perturbation method. Comput Math Appl, 58(11-12):2274-2285.

16. Rivlin, R.S., Ericksen, J.L. (1955) Stress-deformation relations for isotropic materials. J Rat Mech Anal, 4:323-425.

17. Fosdick, R.L., Rajagopal, K.R. (1980) Thermodynamics and stability of fluids of third grade. Proc R Soc Lon A, 339:351-377.

18. He, J.H. (1999) Homotopy perturbation technique. Comput Meth Appl Mech Eng, 178:257-262.

19. Bejan, A. (1995) Entropy generation minimization. CRC Press, New York.

20. Wang, M.C., Guth, E. (1952) Statistical Theory of Networks of Non-Gaussian Flexible Chains. J Chem Phys, 20(7):1144-1157.

21. Flory, P.J., Rehner, J. Jr. (1943) Statistical Mechanics of Cross-Linked Polymer Networks. J Chem Phys, 11:512-520.

22. Treloar, L.R.G. (1946) The statistical length of long-chain molecules. Trans Faraday Soc, 42:77-82.

23. Arruda, E.M., Boyce, M.C. (1993) A three-dimensional model for the large stretch behavior of rubber elastic materials. J Mech Phys Solids, 41(2): 389-412.

24. Bischoff, J.E., Arruda, E.A., Grosh, K. (2002) A microstructurally based orthotropic hyperelastic constitutive law. J Appl Mech, 69:570-579.

25. Kuhl, E., Garikipati, K., Arruda, E.M., Grosh, K. (2005) Remodeling of biological tissue: Mechanically induced reorientation of a transversely isotropic chain network. J Mech Phys Solids, 53:1552-1573.

26. TESTNONLIN.
http://orion.math.iastate.edu/burkardt/f_src/testnonlin/testnonlin.html.

27. Comsol Multiphysics 3.5a Documentations. COMSOL, Inc.

28. Rocha, A., Hahn, M., Liang, H. (2010) Critical fluid shear stress analysis for cell-polymer adhesion. J Mater Sci, 45:811-817.